Nano Energy 57 (2019) 338–352

Contents lists available at ScienceDirect

Nano Energy

journal homepage: www.elsevier.com/locate/nanoen

Full paper

Beyond energy harvesting - multi-functional triboelectric nanosensors on a textile

Tianyiyi He[a,b,c,d,1], Qiongfeng Shi[a,b,c,d,1], Hao Wang[a,b,c,d], Feng Wen[a,b,c,d], Tao Chen[a,e], Jianyong Ouyang[c,f], Chengkuo Lee[a,b,c,d,*]

[a] Department of Electrical & Computer Engineering, National University of Singapore, 4 Engineering Drive 3, 117576 Singapore, Singapore
[b] National University of Singapore Suzhou Research Institute (NUSRI), Suzhou Industrial Park, Suzhou 215123, China
[c] Hybrid Integrated Flexible Electronic Systems (HIFES), 5 Engineering Drive 1, 117608 Singapore, Singapore
[d] Center for Intelligent Sensors and MEMS, National University of Singapore, 4 Engineering Drive 3, 117576 Singapore, Singapore
[e] Jiangsu Provincial Key Laboratory of Advanced Robotics, School of Mechanical and Electric Engineering, Soochow University, Suzhou 215123, China
[f] Department of Materials Science and Engineering, National University of Singapore, 9 Engineering Drive 1, 117575 Singapore, Singapore

ARTICLE INFO

Keywords:
Triboelectric
Self-powered
Textile
PEDOT:PSS
Sensor

ABSTRACT

To accurately evaluate the wellbeing condition of a person, sensing systems with versatile functions are needed. Apart from directly monitoring vital signs, an indirect monitoring approach by measuring human activities with wearable devices has emerged. Herein, a smart textile fabricated with a simple dip coating method is developed with multiple functionalities, such as energy harvesting, physical sensing, and even gas sensing. A maximum output power density of $2\,W\,m^{-2}$ is achieved with a layer of PEDOT: PSS coated textile and PTFE under foot stepping at 2 Hz, and the matched impedance is as low as 14 MΩ. A height-varying multi-arch strain sensor with a large strain sensing range from 10% to 160% is developed. Furthermore, the arch-shaped strain sensors mounted on the human fingers are demonstrated to monitor hand gestures for American Sign Language interpretation and robotic hand control. Additionally, four textile-based sensors located at different body parts are employed to track human activities. Beyond that, the smart textile is also demonstrated to be a building block of a wearable CO_2 sensor. Looking forward, this smart textile could be incorporated into real clothes as both energy harvesters and various functional self-powered sensors to enable smart clothes for healthcare monitoring applications.

1. Introduction

Flexible and wearable electronics have drawn great research interest from the community in the past decades, as revealed by the increasing research and development effort in this area [1–6]. Among them, wearable and flexible sensors with the ability of monitoring daily health status or human activity tracking are of great potential in the home healthcare application. Many studies have been conducted to develop flexible and wearable sensors to monitor healthcare related parameters such as skin temperature [7], electrocardiogram (ECG) [8], chemical contents in body sweat [9], and activity [10], In addition, flexible and wearable sensors are an indispensable part of modern IoT devices due to the advantages of lightweight and user convenience [11–13]. Although the power consumption for each IoT device may be small, the quantity of the sensor nodes in the sensor network could be massive which leads to a large energy expenditure over time. The conventional batteries may not be the optimal choice for the energy source towards the IoT related applications, because of the limited lifetime, high cost of replacement, and potentially hazardous to human health. Therefore, nanogenerators that harvest waste energy from the ambient environment have been developed to provide power for all kinds of wearable sensors. Since mechanical energy is ubiquitously available in the ambient environment, nanogenerators based on the mechanism of piezoelectric [14–20], triboelectric [21–28], and electromagnetic [29,30] have burst out to convert mechanical energy into electricity. Distinguished from others, triboelectric nanogenerator (TENG) has been demonstrated to be a promising approach due to its diverse choice of materials for fabrication, large power density, high

* Corresponding author at: Department of Electrical & Computer Engineering, National University of Singapore, 4 Engineering Drive 3, 117576 Singapore, Singapore.
E-mail address: elelc@nus.edu.sg (C. Lee).
[1] Both authors contributed equally.

https://doi.org/10.1016/j.nanoen.2018.12.032
Received 10 October 2018; Received in revised form 21 November 2018; Accepted 10 December 2018
Available online 18 December 2018

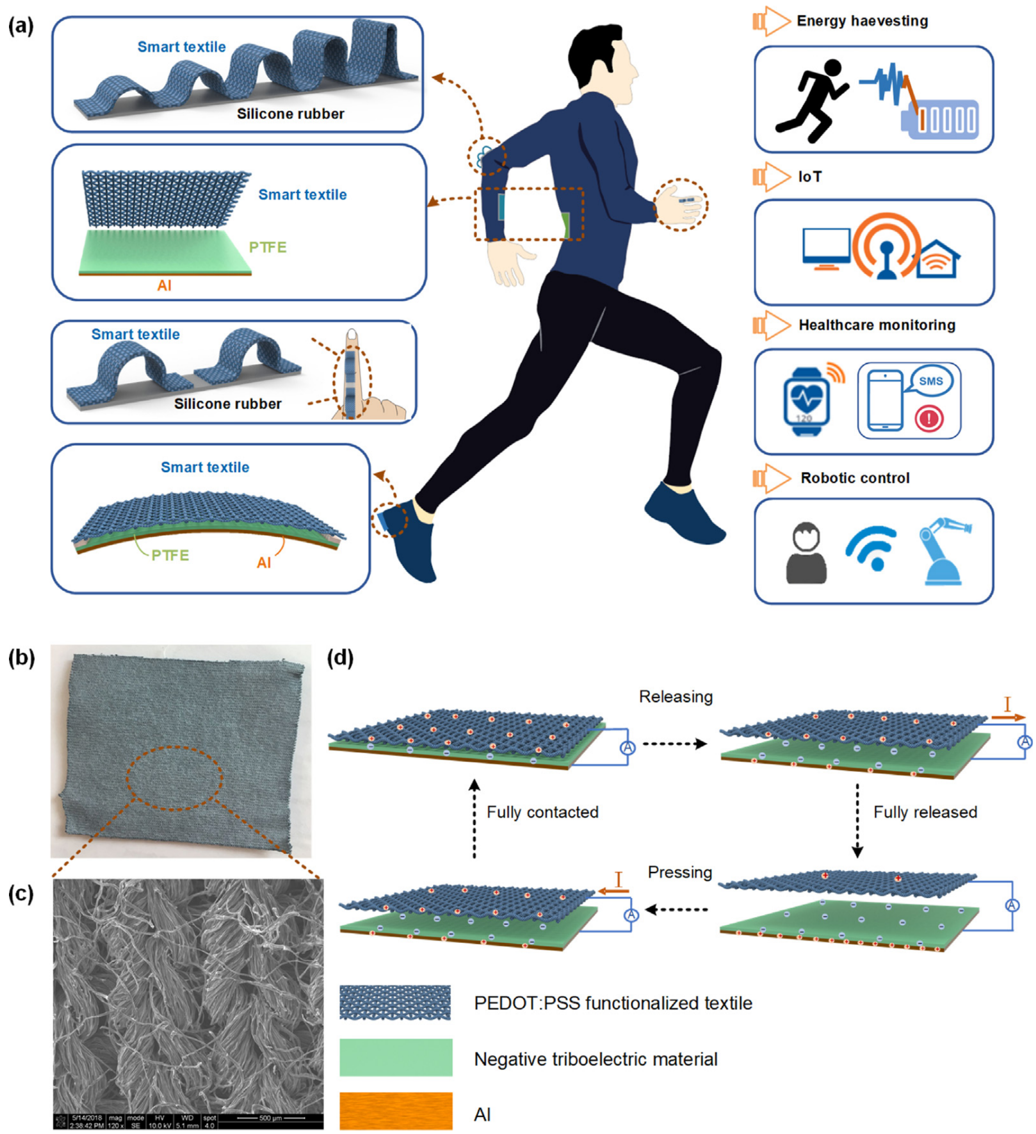

Fig. 1. Device configuration and working mechanism of the smart textile based TENGs. a) Schematic diagrams showing the 3D structures of the versatile textile based TENGs and their applications. b) Photograph of the PEDOT:PSS functionalized cotton textile. c) SEM image of the PEDOT: PSS functionalized textile. d) Working mechanism of the smart textile based TENGs.

efficiency, light-weight, and low-cost [31–35]. Regarding the healthcare and IoT applications, TENG can not only provide sizable output power, but demonstrate novel sensing mechanisms as well, for example, vibration/human motion energy harvesting [36], water wave energy harvesting [37], pressure sensing [38], acceleration sensing [39], finger motion monitoring [40], CO_2 monitoring [41], and direct neural stimulation [42], etc.

Outdoor activity is significant for our health due to various benefits, such as obtaining Vitamin D to maintain cardiovascular fitness and reducing depressive symptoms. Wearable sensors for activity monitoring and human health condition tracking play a vital role towards a healthy way of exercise. Especially, wearable strain sensors located at different body sites can function as an essential part of human activity tracking. One of the common approaches for strain sensing is resistance change measurement, and the sensing range can be broadened to 600% and even 1000% with the aid of carefully designed ultra-stretchable materials [43,44]. Recently, self-powered strain sensors based on TENG have been invented and developed to reduce power consumption of the passive strain sensors. Due to the advantages of universal availability and simple working mechanism, the TENG based strain sensors can be designed into various shapes ranging from thin film structures to fiber structures towards different usage scenarios [45–47].

On the other hand, indoor environment quality is also of great importance especially for home and workplaces, with CO_2 concentration as a key indicator of indoor air quality (IAQ). High CO_2 concentration in atmosphere poses a risk to human health that could lead to permanent brain damage, coma, and even death. So far, TENGs have been adopted as energy sources to power integrated gas sensor [48,49], but only very few research has demonstrated using TENG with functional layer coating for direct gas sensing. For example, a polyaniline nanofiber based TENG has been reported for ammonia sensing [50], and Wang et al. successfully developed a self-powered amenity sensor for CO_2 sensing [41]. These results reveal the feasibility of using triboelectric mechanism for direct gas sensing which provides a solid solution to the challenges of self-powered gas sensors.

Textile, due to its unique properties of soft nature, light weight, wearable convenience, natural micro-structure, and air permeability, is ideally suitable for wearable applications. And the idea of e-textile or smart textile which is endowed with the capability of physical or chemical sensing, signal processing, energy harvesting, and information communication has been proposed years ago [51]. Although the first generation of such smart textile only uses the textile as a substrate for

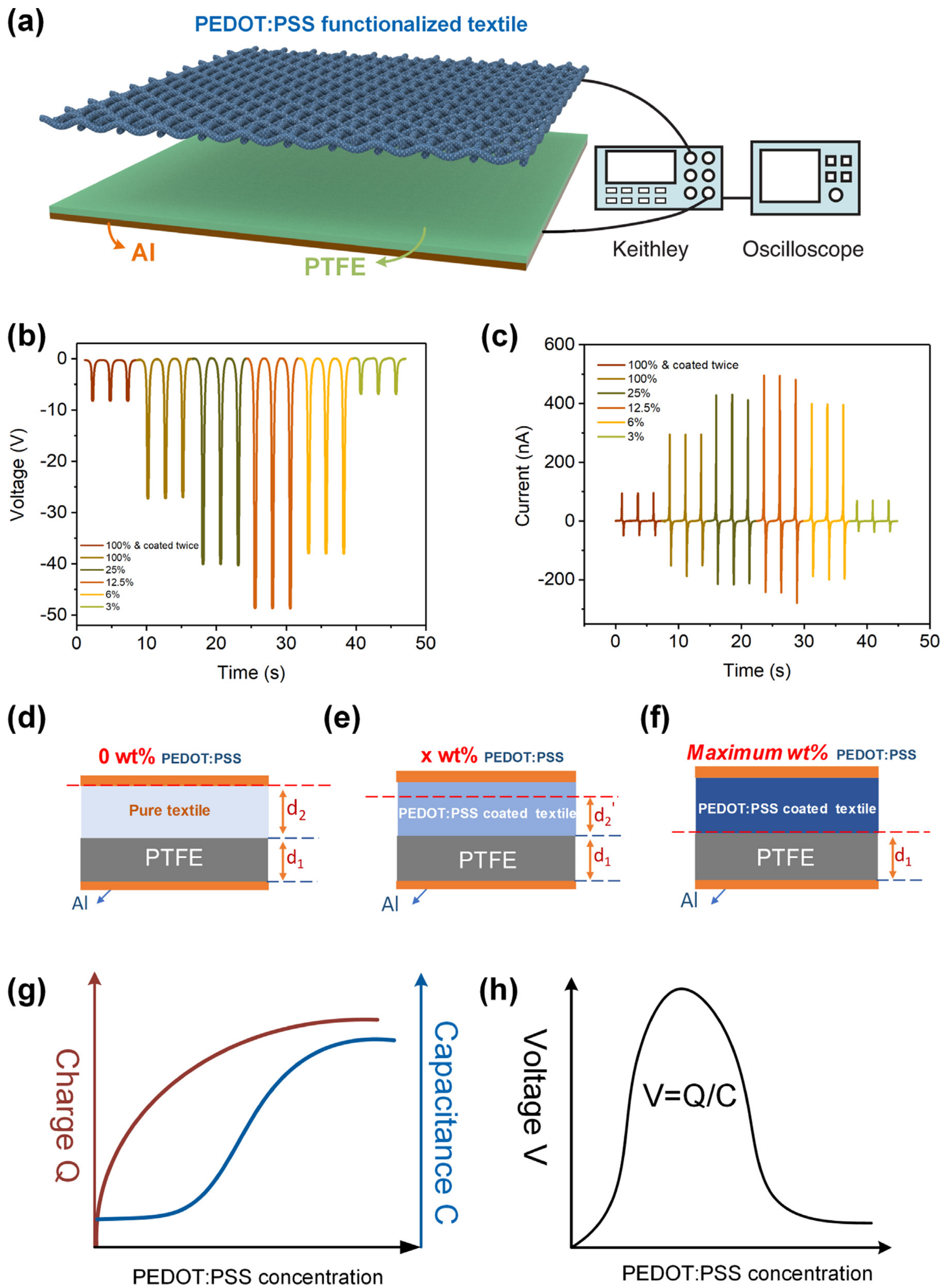

Fig. 2. Triboelectric property characterization of the smart textile based TENGs. a) Schematic diagram of the testing configuration; the PEDOT:PSS functionalized textile is attached on a controllable moving stage, while the Polytetrafluoroethylene (PTFE) thin film with an aluminum electrode is fixed on the static stage aligning with the top textile. b) Real-time output of open-circuit voltages of the six samples with different PEDOT:PSS weight percentages. c) Real-time output of short-circuit currents of the six samples. d-f) The simplified model of the textile based TENG with the PEDOT:PSS weight percentage in textile varying from 0 to a maximum value. g, h) The theoretical changing curve of the transferred charge, the capacitance, and the output voltage of the textile based TENG with the increase of the PEDOT:PSS weight percentage.

rigid and miniaturized electronic components, intrinsically flexible and wearable sensors directly using textile or fabric as functional materials has emerged to realize a seamless integration of the multi-function sensors and textiles. The common sensing mechanism of the textile-based flexible or stretchable physical sensors is based on the resistance or capacitance change which still cannot bypass the essential issue of power consumption [52,53]. To solve this matter, textile-based TENGs have been developed for energy harvesting and self-powered sensing applications. However, the further advancement of the textile-based and self-powered sensor still faces challenges making its way to large-scale production for practical use [45,54–61]. First, a weaving process is inevitable for the fabric-based TENG which is composed of fibers or ribbons. This could largely boost the complexity and cost of the fabrication. Second, the reported fabric-based TENGs usually face the limitations such as low stretchability, complicated fabrication process, and low wearing comfortability. Third, the current textile-based TENGs typically target a single usage scenario corresponding to a single or few similar body parts. Preferably, the wearable sensors should be able to form a sensing system that can respond to multiple forms of mechanical stimuli form different body parts, such as pressing, sliding, stretching, and bending. More importantly, the textile-based TENG exhibits great potential for gas sensing due to the large surface area and gas permeability, but it has not been reported for this application yet.

Herein, we propose smart textile-based triboelectric nanogenerators with versatile configurations towards diversified applications including energy harvesting, internet of things (IoT), healthcare monitoring, and robotic control as illustrated in Fig. 1(a). A simple and low-cost dip coating approach is proposed to fabricate the PEDOT:PSS functionalized textiles. This simple and low-cost process can be readily adapted for large-scale fabrication of the functionalized textiles. The energy harvesting property under different human motions of the functionalized textile based TENG has been thoroughly investigated. Thereafter, a multi-arch strain sensor based on PEDOT:PSS functionalized textile with a large sensing range has been fabricated. Next, the arch-shaped strain sensors are mounted on finger joints to function as finger bending sensors for American Sign Language interpretation and robot finger control (e.g., perform different hand gestures, grab items, and play piano). Moreover, with the aid of polyethylenimine (PEI) coating on the PEDOT:PSS/textile composites, a smart textile for CO_2 sensing has been developed.

2. Triboelectric property of the smart textile

Poly (3,4-ethylenedioxythiophene): poly (styrene sulfonate) (PEDOT:PSS) is one of the most successful conducting polymers in terms of practical applications that has been thoroughly investigated in the past decades [62–64]. It possesses many unique properties, such as good film-forming ability by versatile fabrication techniques, superior optical transparency in visible light range, high electrical conductivity, intrinsically high work function and good physical and chemical stability in the air [65]. Ding et al. reported a stretchable and conductive textile fabricated simply by soaking the textile in PEDOT:PSS solution [66]. With the coating process, the textile not only becomes conductive but also is endowed with properties of PEDOT: PSS, which has a great potential for versatile applications such physical sensing or energy harvesting. Similarly, Pu et al. reported a fabric TENG composed of conductive textiles which were coated with metal Ni [60]. Compared to the Ni coating, the simple and scalable PEDOT:PSS coating induced soft and stretchable conductive textile is highly suitable to be the building block of the textile-based TENGs.

The facile and low-cost PEDOT:PSS coating approach is adopted to fabricate a smart textile for both energy harvesting and sensing. Considering the advantages of soft, lightweight, tough, gas permeable, and easily available in the market, pure cotton textile, i.e, 100% cotton, is used as the substrate for the smart textile. The smart textile in Fig. 1(b) is fabricated by immersing a piece of cotton textile in PEDOT:PSS solution. The SEM image of the PEDOT:PSS functionalized textile is shown in Fig. 1(c). The cotton textile becomes conductive owing to the PEDOT:PSS coating and its conductivity can be adjusted in a wide range with varying PEDOT:PSS concentration.

PEDOT:PSS is extensively used in all kinds of flexible electronic devices and it is also implemented in flexible or stretchable TENG as electrodes to collect electrons [67,68]. However, as a potential material for both triboelectric charge generation and collection, the triboelectric property of PEDOT: PSS has never been thoroughly discussed. To investigate the PEDOT: PSS concentration on the triboelectric property of the smart textile, six samples of the smart textile of varying PEDOT:PSS concentrations were fabricated using the same dip coating method with coating solutions containing different weight percentages of the PEDOT:PSS solution. Fig. 1(d) demonstrates the working mechanism of the PEDOT:PSS functionalized textile-based TENGs, in which a thin film of PTFE with an aluminum electrode attached on the back works as the negative triboelectric layer. Before the coating process, the as-purchased PEDOT: PSS solution was doped with 5 wt% DMSO solution first to further improve its conductivity, and then the doped PEDOT:PSS solution was diluted by different ratio DI water. The details of the coating solutions corresponding to the six samples are illustrated in Table S1 (Supporting Information). Distinguished from others, sample 1 was coated twice with non-diluted doped PEDOT:PSS solution. After dilution, the pure cotton textile was immersed in the coating solution for 10 min for full absorption. Then the wet textile was put into an oven and baked for at least 30 min at 80 °C until it was fully dried.

The testing configuration for the characterization of the open-circuit voltage (V_{OC}) and short-circuit current (I_{SC}) is demonstrated in Fig. 2**(a)**. The applied force and frequency for the repetitive movement of the moving stage are set at 10 N and 0.5 Hz. The size of each textile sample and PTFE thin film is fixed at 5 cm × 5 cm. The real-time output of V_{OC} and I_{SC} of the six samples are depicted in Fig. 2(b) and (c). More specifically, the histograms of the triboelectric output of six samples are sketched in Fig. S1(a) and (b) (Supporting Information). It can be observed that both triboelectric outputs increase with the descending of PEDOT:PSS concentration up to a certain range and then decrease. A highest open-circuit voltage of 49.7 V and a largest short-circuit current (peak to peak value) of 787 nA can be observed in sample 4, which is coated with a coating solution containing 12.5 wt% of PEDOT:PSS solution.

This non-monotone relationship between the triboelectric output and the PEDOT:PSS concentration could be explained by the combination of the conductivity of the textile and the capacitance of the TENG. Since the triboelectric charges are only generated on the contact surface, a simple assumption could be made that the contact surface of the textile is fully covered by PEDOT:PSS and the generated triboelectric surface charge remains the same amount as long as the PEDOT:PSS concentration is not zero. In this case, even if the PEDOT:PSS weight percentage of the textile decreases, the amount of the triboelectric charges on the contact surface should maintain the same. However, a lower PEDOT:PSS concentration in textile leads to less conductive paths in the fabric network, which means the efficiency of the charge transfer of the functionalized textile is reduced. Therefore, the transferred charge Q that gives rise to triboelectric output increases with PEDOT:PSS concentration in textile. In other words, a higher PEDOT:PSS concentration in textile leads to a higher conductivity of the textile, which could largely improve the charge transfer efficiency during the contact-separation process. Accordingly, the estimated changing curve of the transferred charge over PEDOT:PSS concentration is drawn in Fig. 2(g).

To understand the TENG capacitance change with the increasing PEDOT:PSS concentration, a simplified model of the PEDOT:PSS functionalized textile based TENG is depicted in Fig. 2(d–f). When the PEDOT:PSS weight percentage is zero, the functionalized textile is just a pure cotton textile, and the TENG at the fully contacted condition could equal to a capacitor as shown in Fig. 2(d), where the dielectric of the capacitor contains not only the PTFE thin film but also the textile. The permittivity and the thickness of the PTFE are constant values, therefore, the capacitance over the PTFE thin film (C_{PTFE}) should also be a constant. Here the overall capacitance of the TENG is considered as a sum capacitance of two series-connected capacitors. Due to the principle of series-connected capacitors, the overall capacitance at this condition should be smaller than C_{PTFE}. Therefore, the capacitance of the TENG now is the smallest. While the textile is equivalent to a highly conductive electrode in another extreme condition where the PEDOT:PSS concentration of the textile reaches its highest value, the dielectric of the capacitor only contains the PTFE thin film, and hence the capacitance reaches its maximum value at C_{PTFE}. At any in-between condition where the PEDOT:PSS weight percentage is non-zero, the dielectric contains both PTFE thin film and part of the textile. At this point, the capacitance value is between the maximum and minimum values in the previous two extreme conditions. Hence the capacitance of the TENG should increase with the PEDOT:PSS concentration in textile as illustrated in Fig. 2(g).

Briefly speaking, both transferred charge and the TENG capacitance increase with PEDOT:PSS concentration. Besides, the gradient of the transferred charge over PEDOT:PSS concentration curve decreases with the concentration; while the gradient of the capacitance-PEDOT:PSS concentration curve increases with the concentration. Therefore, the voltage of the TENG which equals the ratio of transferred charge over

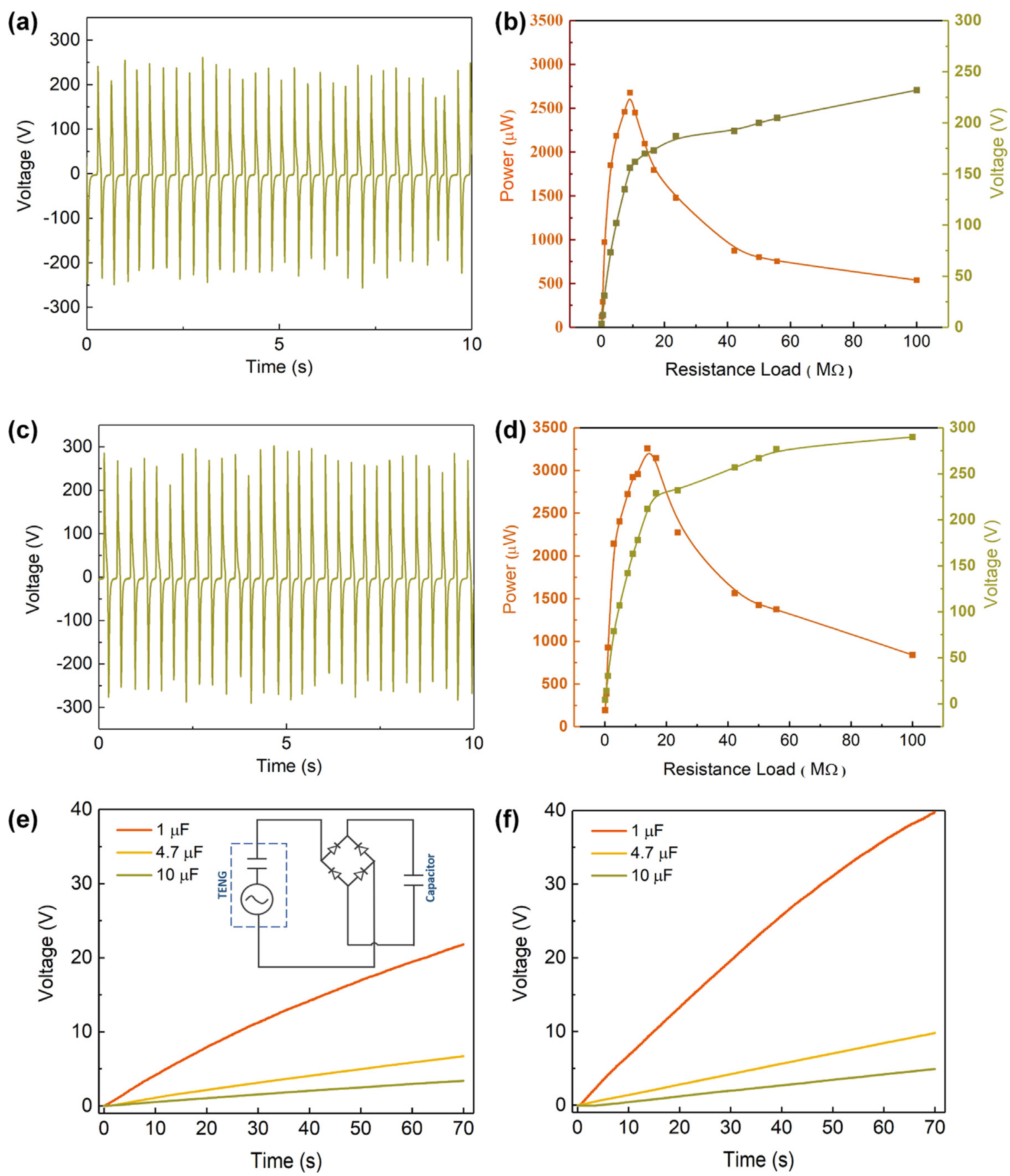

Fig. 3. Energy harvesting from different body motions with the PEDOT:PSS functionalized textile based TENG. a, c) Real-time output voltage on a 100 MΩ load resistor with hand tapping and foot stepping. b, d) Power curve of the textile-based TENG with under different loads from hand tapping and foot stepping motions. e, f) The changing curve of various capacitors with the textile-based TENG under hand tapping and foot stepping; the inset shows the circuit connection for the capacitor charging.

capacitance follows the trend as shown in Fig. 2(h). This theoretical curve well fits with the experimental data as shown in Fig. 2(b). To further confirm this proposed theory, the impedance and sheet resistance of four samples with varying PEDOT:PSS concentrations are measured as shown in Fig. S1(c) and (d) (Supporting information). As known to all, there is a negative correlation between the impedance and the capacitance of the TENG, hence the histogram of the impedance of the four samples in Fig. S1(c) (Supporting information) well demonstrates that the capacitance increases with the PEDOT:PSS concentration. Similarly, as depicted in Fig. S1d (Supporting information), the sheet resistance of the textile decreases with PEDOT:PSS concentration, which will lead to a higher amount of transferred charge. In short, the combination of the varying conductivity and the TENG capacitance gives rise to the non-monotone relationship between the triboelectric output and the PEDOT:PSS concentration. Moreover, the optimal concentration of PEDOT:PSS in the functionalized textile is investigated. To be more specific, the PEDOT:PSS functionalized textile should obtain the highest triboelectric property when the corresponding coating solution contains 12.5 wt% PEDOT:PSS solution.

3. Energy harvesting with the smart textile

According to the characterization part, all the textiles for energy harvesting are fabricated by the coating solution containing 12.5 wt% PEDOT:PSS solution to achieve the best performance. To investigate the energy harvesting property from different body motions of the PEDOT:PSS functionalized textile based TENG, triboelectric outputs from simple hand tapping and foot stepping have been investigated with the same device configuration and the photographs of the devices are shown in Fig. S2 (Supporting information). The PEDOT:PSS functionalized textile works both as the positive triboelectric layer and the electrode, and the PTFE thin film is used to generated negative charges. The size of the textile and PTFE thin film are both 4 cm by 4 cm. The hand is moving up and down repeatedly with a frequency of 2 Hz. The output voltage collected from this tapping motion with a 100 MΩ probe is depicted in Fig. 3**(a)**. The corresponding power curve under different loads of this textile-based TENG is depicted in Fig. 3(b). An average of 460 V peak to peak voltage can be generated through the hand tapping, and a maximum output power of 2.67 mW is measured with a load resistance of 9 MΩ. Similarly, the textile and the PTFE thin film are attached to a Polyethylene terephthalate (PET) confinement structure as shown in Fig. S2(b) (Supporting information). This TENG is then put beneath the human shoe to harvest energy from foot stepping. The foot moves up and down with the same frequency of 2 Hz. The real-time output voltage and the power curve under different loads are shown in Fig. 3(c) and (d). Owing to the larger force that the foot applied on the TENG, a higher peak to peak voltage of 540 V is collected. Besides, the TENG works under this condition can also achieve a higher maximum output power of 3.26 mW with an external resistance of 14 MΩ. To study the durability of the PEDOT: PSS coated textile, the textile-based TENG is tested through a repetitive contact-separation motion for 4 h with a fixed frequency of 2 Hz and force of 40 N, and the results are depicted in Fig. S3. It can be observed that the output voltage of the textile-based TENG shows almost no degradation after 4 h of repetitive contact-separation motions (roughly 7200 times), which has well indicated a great durability of the PEDOT: PSS coated textile. The washability of the PEDOT:PSS functionalized textile is also investigated. The open-circuit voltage is measured each time after the textile washed in water with an ascending wash strength. After the fifth wash where the textile is strongly rubbed with another piece of textile for five minutes, the open-circuit voltage can still maintain 81% of its original value as shown in Fig. S4 (Supporting information).

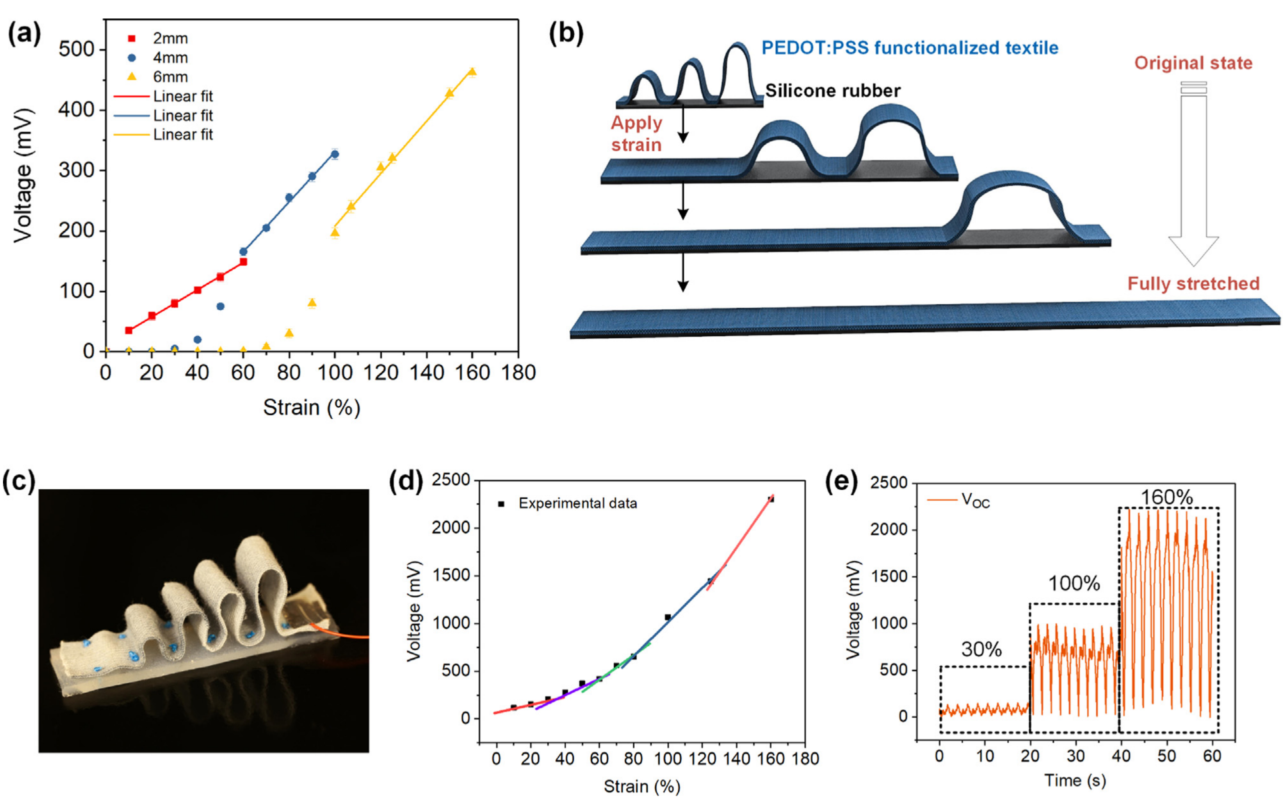

Fig. 4. Characterization of the single-arch strain sensors and the height-varying multi-arch strain sensor. a) The open-circuit voltage of the single-arch strain sensors with different applied strain when the arch height is 2 mm, 4 mm, and 6 mm respectively. b) Schematic illustration of the shape changing process when a height-varying three-arch strain sensor is applied with a consecutive strain. c) Digital photo of the height-varying multi-arch strain sensor. d) The open-circuit voltage of the height-varying multi-arch strain sensor with different strain from 10% to 160%. e) Real-time output of the height-varying multi-arch strain sensor with the applied strain of 30%, 100%, and 160%.

Previously, a wrinkled PEDOT:PSS film based TENG was developed to harvest human mechanical energy, but the peak output power density was only 0.406 μw cm^{-2} [67]. A single thread based TENG for wearable applications was demonstrated and it was able to achieve a peak output power of 74 μW cm^{-2} when the external resistance was 1 MΩ [54]. Although the impedance of the TENG was as low as 1 MΩ, still the output power density was not very high. Xiong et al. reported a wearable all-fabric-based TENG for water energy harvesting, and it can generate an output power density of 14 μW cm^{-2} from mechanical energy of water at a load resistance of 100 MΩ [59]. For our textile based TENG, a high peak output power density of 203.75 μW cm^{-2} or 2 W m^{-2} can be achieved from foot stepping at a load of 14 MΩ.

The energy generated from different body motions can also be stored for further use. Fig. 3(e) and (f) show the charging curves of the commercial capacitors with varying capacitances. The circuit connection is depicted as the inset of Fig. 3(e). For the hand tapping motion with a frequency of 2 Hz, the charging curves of capacitors with the capacitance of 1 μF, 4.7 μF, and 10 μF are illustrated in Fig. 3(e). To a 1 μF capacitor, the charged voltage can reach up to 19 V in around 60 s. For a capacitor with a capacitance of 10 μF, it can be charged up to 3 V in around 60 s. In Fig. 3(f), the charging curves under foot stepping with 1 μF, 4.7 μF, and 10 μF capacitors are also depicted. Since foot stepping gives a larger contact force and thereby a higher output voltage, the gradients of the charging curves are higher than the ones under hand tapping. To the 1 μF capacitor, the charged voltage can reach up to 36 V in around 60 s. The 10 μF capacitor can be charged up to 4.4 V in around 60 s. The stored energy from either hand tapping or foot stepping can then be used as a power source to drive low power consumption electronics for diversified applications.

4. Strain sensor for finger bending sensing and robotic control

4.1. Height-varying multi-arch strain sensor

Human activity tracking towards healthcare monitoring typically requires wearable strain sensors located at different body parts to record the body motions at any time. The emerging TENG has provided a solid solution to the challenges of self-powered strain sensors. The PEDOT:PSS functionalized textile is soft, light-weight, and stretchable that can be made into various shapes and it is highly desirable to be the building block for wearable strain sensors towards the activity monitoring application. To transfer strain into the contact-separation process to generate a triboelectric output, here we propose a height-varying multi-arch strain sensor based on the PEDOT: PSS

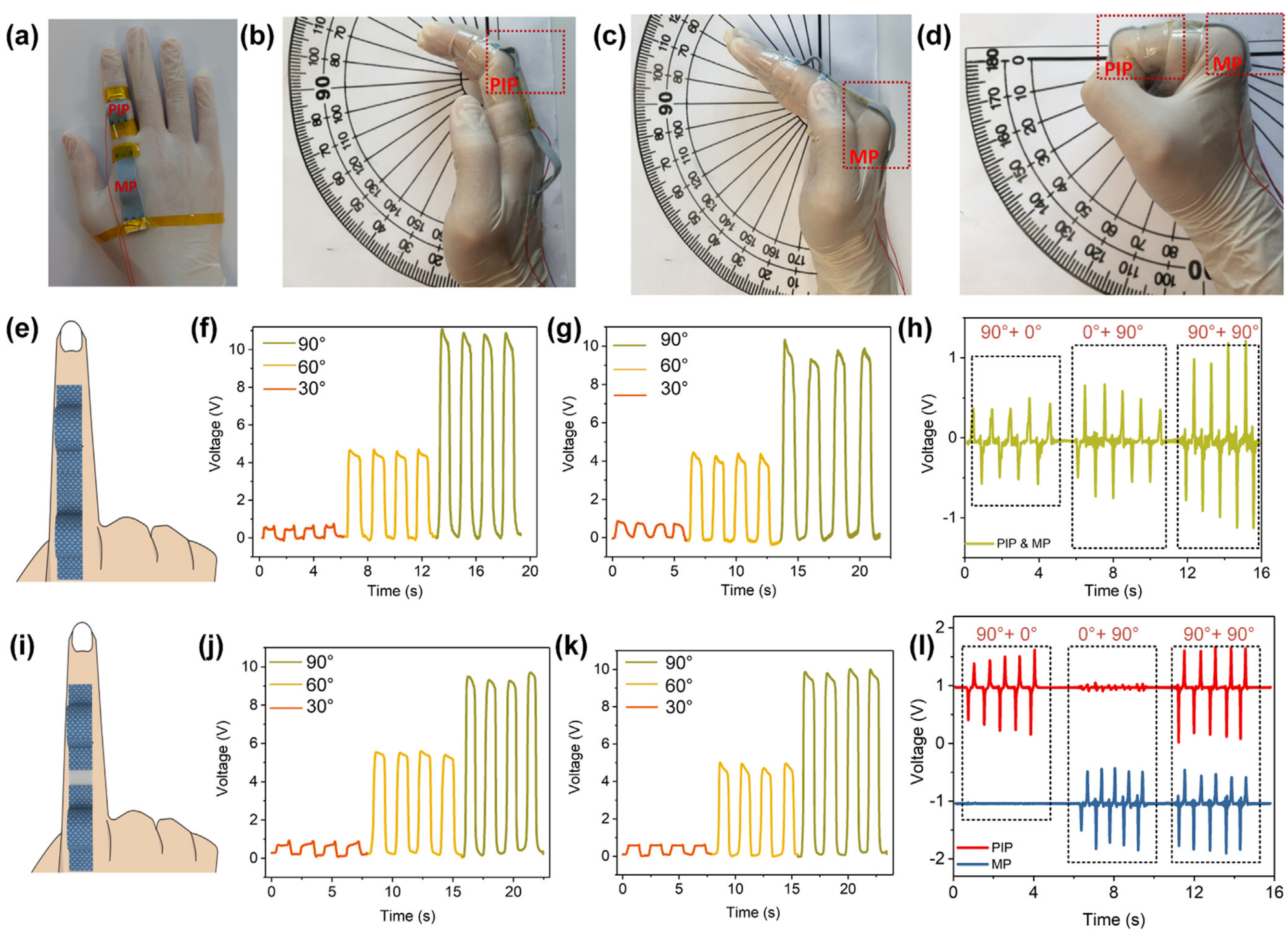

Fig. 5. Characterization of the arch-shaped finger bending sensor. a) Photos of the two-arch finger bending sensor mounted on the PIP joint and MP joint. b-d) Photographs of the PIP bending at 60°, the MP bending at 60°, and the two joints bending at 90° together. e) Schematic illustration of the two-connected-arch finger bending sensor. f) The measured open-circuit voltage with the PIP bending at 30°, 60°, and 90°. g) The measured open-circuit voltage with the MP bending at 30°, 60°, and 90°. h) The output voltage measured by the 100 MΩ probe when two joints move in the following sequence: only the PIP bends at 90⁰, only the MP bends at 90°, and the two joints bend at 90° simultaneously. i) Schematic illustration of the two-separated-arch finger bending sensor. j) The open-circuit voltage from the arch on top of the PIP when it bends at 30°, 60°, and 90°. k) The open-circuit voltage from the other arch mounted on the MP when it bends at 30°, 60°, and 90°. l) The output voltages from two separated arches recorded with the 100 MΩ probe when the PIP bends at 90° solely, the MP bends at 90° solely, and the two joints bend at 90° simultaneously.

functionalized textile as demonstrated in Fig. 4(c). The textile is fabricated with the same dip coating process as what has mentioned in the previous part. The coating solution contains 12.5 wt% of PEDOT: PSS solution to achieve the highest triboelectric output. Silicone rubber, which is a highly stretchable and negative triboelectric polymer, is used for the bottom layer to provide negative charges. The working mechanism is depicted in Fig. S5 (Supporting information).

Compared to a consistent-height multi-arch strain sensor, this height-varying multi-arch design should give rise to a wider sensing range from small strain to large strain. Firstly, three single-arch based strain sensors with different arch heights are fabricated and tested, and the measured open-circuit voltages are depicted in Fig. 4(a). The length and width of the three sensors are fixed at 1 cm and 1.5 cm with arch heights of 2 mm, 4 mm, and 6 mm, respectively. A controllable linear motor is used to give a repetitive strain to the strain sensor as shown in Fig. S6 (Supporting information). Theoretically, for the single arch structure, the voltage generated is only in linear with the applied strain in a certain range where the arch is stretched to a very low curvature shape. The detailed explanation is provided in Fig. S7 (Supporting information). Therefore, only a limited effective sensing range is observed for each single-arch strain sensor in Fig. 4(a), and the output beyond this range is much smaller and non-linear with the applied strain. At 100% strain, the 4 mm strain sensor is stretched to its maximum elongation and the textile is in fully contact with the silicone rubber film; while for the 6 mm single-arch strain sensor, it just reaches its linear range where the textile is close but not in fully contact with the silicone rubber film. Hence the output voltage of the 6 mm height sensor is lower than the 4 mm sensor at 100% strain. The results reveal the limitation of the single-arch or consistent-height multi-arch design in terms of wide strain sensing range.

To realize a large and continuous strain sensing range, here we combine the arches with varying heights together as shown in Fig. 4(c). The height of each arch is 2 mm, 4 mm, 6 mm, 9 mm, and 12 mm respectively. The length and width of each arch are the same as previous sensors, 1 cm, and 1.5 cm. A three-arch model is drawn to illustrate the shape changing process of the height-varying multi-arch strain sensor in Fig. 4(b). With an ascending strain applied, the three arches will be stretched to be flat one by one, hence each arch dominates the triboelectric output in three successive ranges which is their corresponding linear sensing range. Accordingly, there will be discontinuities between each linear sensing range due to the contact area difference among the textile arches. Here this height-varying multi-arch strain sensor is also attached to the movable stage for the characterization with a moving frequency of 0.5 Hz. The real-time output of this multi-arch strain sensor under 30% strain, 100% strain, and 160% strain is depicted in Fig. 4(e). In Fig. 4(d), the open-circuit voltage versus applied strain of the multi-arch strain sensor is depicted. It can be observed that the open-circuit voltage is in a good linear relationship in five regions due to the five arches. Hence the height-varying multi-arch strain sensor has been demonstrated to be able to detect strain over a wide range even though with a sacrifice in the linearity over the whole sensing range. Previously, a stretchable self-powered strain sensor was developed by coiling a fiber-based TENG around a stretchable silicone fiber, but the detection strain was only up to 25% [69]. Distinguished from others, a digitalized self-powered strain gauge was demonstrated with good accuracy, sensitivity, and linearity. However, its sensing range was still limited to 40% and the size especially the length of the strain gauge was quite large due to the unique IDT design of the electrodes [46]. For human activity monitoring or tracking, a strain sensor with a wider sensing range is essential because the strain variation of some body parts such elbow or knee could be quite large during activities. Furthermore, in the scenarios where extremely-large strain sensing is required, the sensing range of the multi-arch strain sensor can be further broadened by assembling more arches with higher heights.

Besides triboelectric output measurement, resistance change characterization is a common sensing mechanism for most of the strain sensors, and textile coated with conductive nanoparticles is also a common configuration for a wearable strain sensor [70]. A PEDOT:PSS coated textile strip with 1 cm width and 2 cm length is characterized as well. The resistance of the strip under different strain is measured and depicted in Fig. S8 (Supporting information). A good linear response from 5% to 20% strain is observed, but the largest strain that is can withstand is only 35% due to the limited elongation of the textile structure. For an applied strain of 20%, the relative resistance change of the textile strip is $\Delta R/R_0 = 45\%$, where R and R_0 are the resistance with and without applied strain and $\Delta R = |R\text{-}R_0|$.

4.2. Arch-shaped finger bending sensor

Wearable strain sensors can function as interfaces between human motion and electric signal to control and operate electronic devices towards diversified applications. Here we fabricated a two-arch strain sensor for finger motion detection as shown in Fig. 5(a). This strain sensor is constructed by PEDOT: PSS functionalized textile strips and a silicone rubber thin film. Each arch sits right above one finger joint to sense the bending movement of this finger joint. The proximal interphalangeal joint (PIP) and the metacarpophalangeal joint (MP) of the index finger are marked in Fig. 5(a). Two configurations with the same arch structures are investigated, one with two connected arches as illustrated in Fig. 5(e) and the other one with two separated arches as shown in Fig. 5(i). The width of all the arches stays the same at 1.5 cm, while the length of the arch located at the PIP or the MP is 2 cm and 4.5 cm, respectively. The arch height on top of the PIP is 0.8 cm and the arch located at the MP is 1.2 cm high. The finger bending sensor is attached to the human index finger for characterization. Fig. 5(b) shows the sole movement of the PIP at a bending angle of 60 degrees, while Fig. 5(c) demonstrates the single movement of the MP at a bending angle of 60 degrees. In Fig. 5(d), the PIP and MP bend at 90 degrees at the same time.

The open-circuit voltage of the strain sensor in Fig. 5(e) under different finger motions is plotted in Fig. 5(f-g). Here the frequency for the bending movement is approximately 0.5 Hz. When the PIP bends at 30 degrees, 60 degrees, and 90 degrees while the MP stays still, the open-circuit voltage is measured and plotted in Fig. 5(f). When the MP bends at 30 degrees, 60 degrees, and 90 degrees while the PIP is static, the open-circuit voltage is plotted in Fig. 5(g). In Fig. 5(h), the output voltage of the strain sensor on a 1 MΩ resistor is measured when three different motions are applied to the strain sensor: only PIP bends at 90 degrees; only MP bends at 90 degrees; PIP and MP bend at 90 degrees at the same time. From the output signal, we can clearly identify the bending angle of each finger joint when they move separately. However, as shown in Fig. 5(h), from one output we cannot determine which joint is bending and detect the bending angles of each joint when the PIP and MP are moving together.

To decouple the two parameters, the finger bending sensor with separated arches is fabricated as demonstrated in Fig. 5(i). Each arch produces a triboelectric output separately, which means that one output is for sensing the motion of the PIP and another one is for movement detection of the MP. The open-circuit voltage of this finger bending sensor where only the PIP is bending at 30 degrees, 60 degrees, and 90 degrees is plotted in Fig. 5(j). And the open-circuit voltage coming from another arch where just the MP is bending at 30 degrees, 60 degrees, and 90 degrees is depicted in Fig. 5(k). Each arch structure is able to well identify the bending angles of the corresponding finger joint. Besides, the output voltages of the two arches on a 1 MΩ resistor when the PIP or the MP bends at 90 degrees separately and when they bend at 90 degrees at the same time are plotted in Fig. 5(l). It can be easily differentiated from the two output voltages between the two finger joints when the PIP and MP bend together. Furthermore, the amplitude of the open-circuit voltage of each arch reveals the bending angle of each finger joint. In short, two separated arches are beneficial in precisely identifying the finger movement for sensing and control.

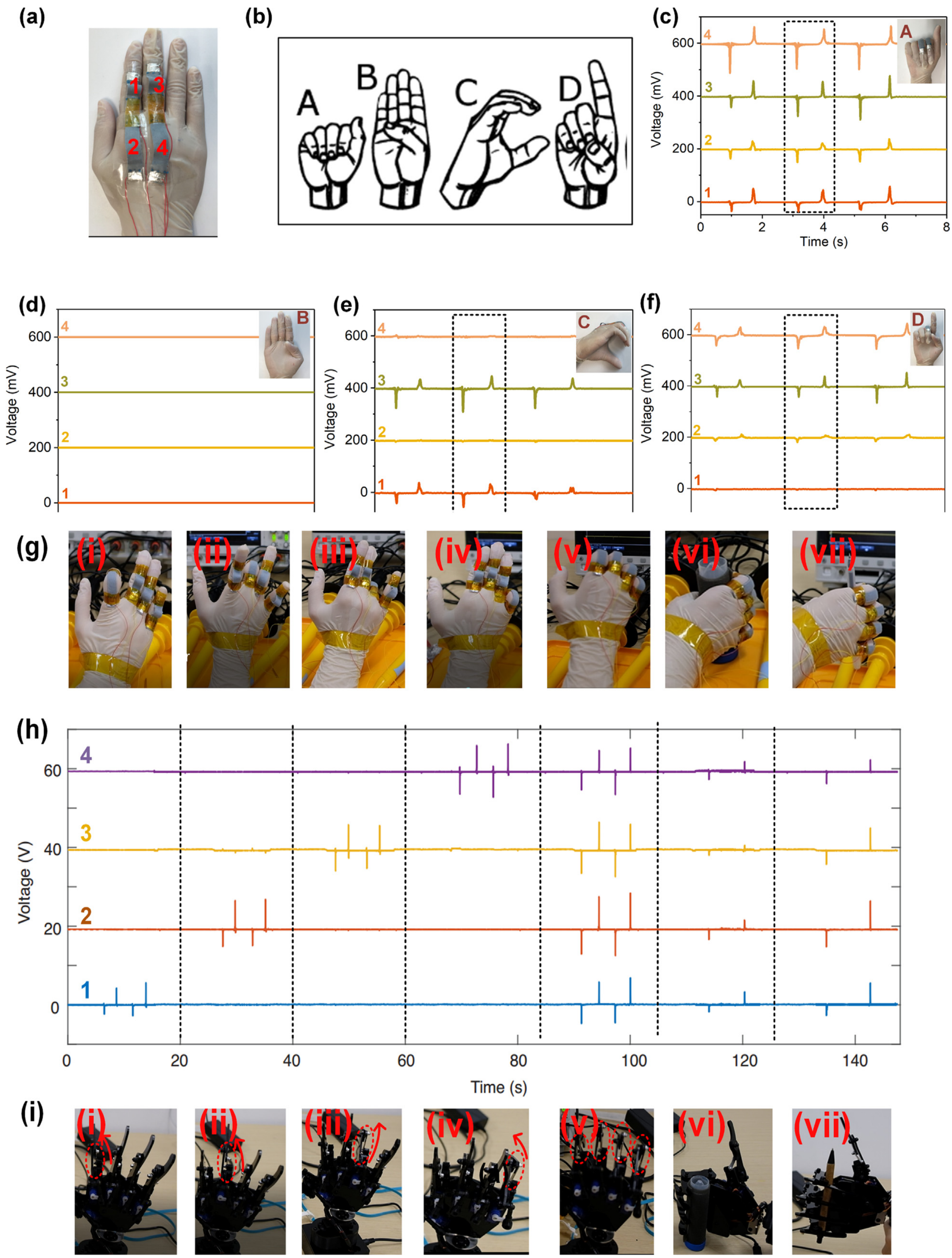

(caption on next page)

Fig. 6. Hand gesture capture and robotic hand control with the finger bending sensors. a) The photographs of the two-arch finger bending sensors attached to the index finger and the middle finger. The four arches are labelled from 1 to 4 in accordance with channel 1–4. b) Illustration of the hand gestures representing alphabet from "A" to "D" in American Sign Language. c–f) Output voltages from the four arches when the hand duplicates the gestures representing alphabet from "A" to "D". The black dot line marks the signal in one cycle of the movement. g) Photographs of seven different hand motions: bending one of the fingers at 90 degrees, bending four fingers together at 90 degrees, grabbing a bottle of a large diameter, and grabbing a pen of a small diameter. h) The output voltages of the four arch-shaped finger bending sensors. Channel 1–4 are in accordance with the motions of the index finger, the middle finger, the ring finger, and the pinkie. To put the output voltages of the four channels into one graph, a bias of 20 V, 40 V, and 60 V is applied to channel 2, channel 3, channel 4 separately. i) The photos of the robotic hand gestures corresponding to the seven different hand motions.

4.3. Hand motion capture

Using the optimized finger bending sensor, we first demonstrate its application in hand motion capturing. Here we attached the two-arch finger bending sensors to both the index and the middle finger shown in Fig. 6(a). To make it more clear, the four arches are labelled from one to four based on their sites on finger joints as demonstrated in Fig. 6(a). The four hand motions which represent four alphabet signs in the American Sign Language with different bending angles of the index and middle fingers are shown in Fig. 6(b). Fig. 6(c–f) illustrate the real-time response from the four arches corresponding to each hand motion as demonstrated in Fig. 6(b). Each output signal is associated with the movement of one finger joint. A video demo of hand gesture monitoring can be found in Video 1 (Supporting information). For the sign of alphabet "A" where all the PIPs and the MPs are bending at 90 degrees, the open-circuit voltages of the four arches reach their maximum as plotted in Fig. 6(c). The sign of alphabet "B" involves no movement of the index and middle fingers, resulting in no output in four channels as depicted in Fig. 6(d). To show the sign of alphabet "C", only the PIPs of the index finger and middle finger need to bend at a certain angle. Hence there are only two observable output voltages in channel 1 and 3 as shown in Fig. 6(e), which is corresponding to the arch 1 and the arch 3. For the sign of alphabet "D" where only the PIP and MP of the middle finger bend at the same time and the whole index finger stays still, only two observable output voltages coming from channel 3 and 4 which associate with arch 3 and 4 on the middle finger. A tiny output voltage in channel 2 is also generated during this motion because the movement of the MP of the middle finger could lead to a slight shift of the MP of the index finger due to their physical connection in hand. In summary, from the output voltages of the four arches, we are able to identify the movements of the index finger and the middle finger detailing to each joint of the two fingers. Furthermore, there is a potential to detect and discriminate more complicated hand gestures by adding in more sensing elements attached to other finger joints.

4.4. Robotic hand control

In the previous part, we have demonstrated the practicability of using the arch-shaped finger bending sensor for hand-motion detection. Here we have further explored its possibility of the sensing signal for

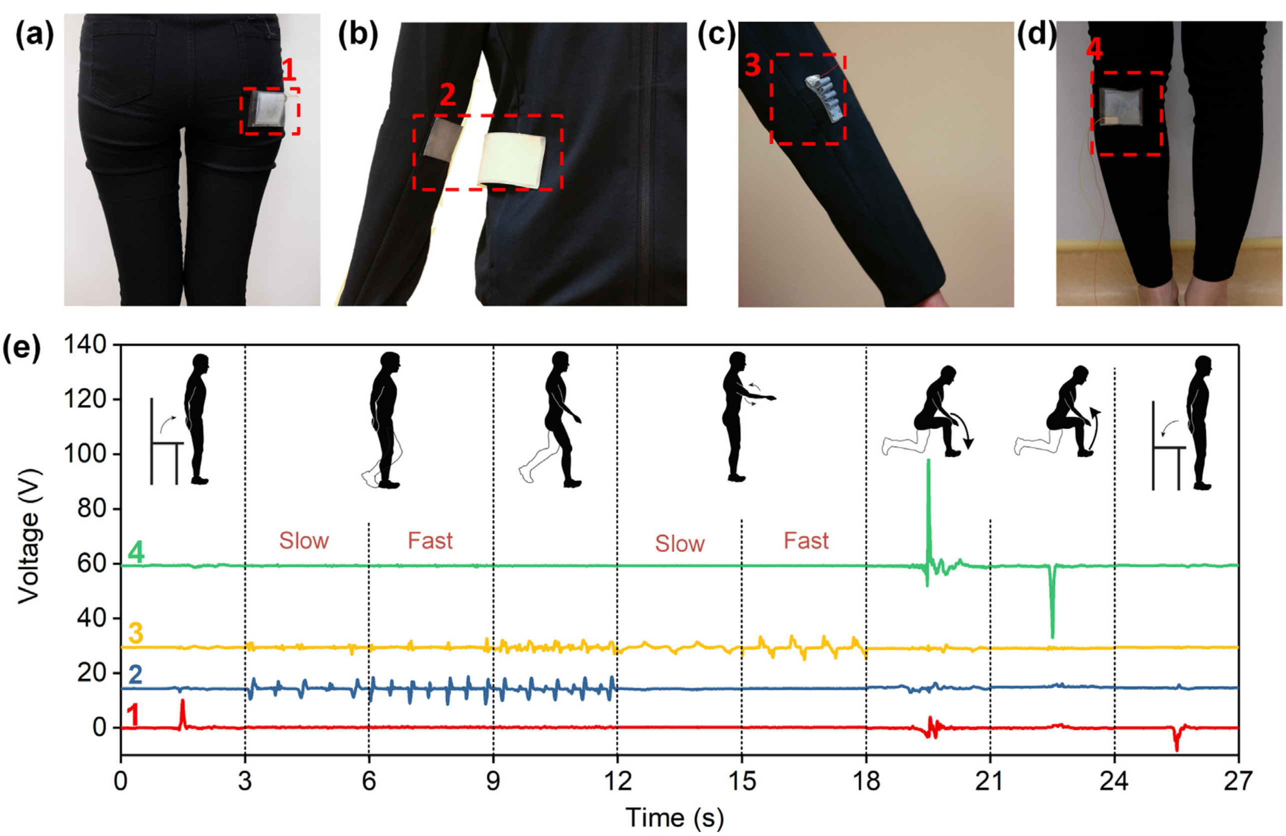

Fig. 7. Human activity monitoring with the textile-based TENGs. a-d) Photographs of the four devices attached to different body parts which are labelled from 1 to 4 corresponding to channel 1 to channel 4. a) A simple three-layer TENG based on the smart textile attached to an arched PET confinement structure on the hip. b) A textile-based TENG attached on the sleeve and underneath the arm separately. c) The height-varying multi-arch strain sensor on the elbow. d) A three-layer TENG based on the smart textile attached to an arched PET confinement structure beneath the knee. e) The output voltages of the four devices when the person is standing up, slowly walking, fast walking, running, slowly bending arm, fast bending arm, falling down, getting up, and sitting down. To put the output voltages of the four channels into one graph, a bias of 15 V, 25 V, and 60 V is applied to channel 2, channel 3, channel 4 separately.

robotic hand control. Since the robotic hand only has one joint at each finger, the one-arch finger bending sensors are fabricated and mounted on top of each PIP joint to detect the bending motion of the index finger, middle finger, ring finger, and the pinkie. The size of the four arches is the same with the arch on top of the PIP in previous sections. The output signal from each sensor is recorded and processed to control the movement of the robotic hand. Fig. 6(g) and (i) demonstrate the gestures of the human hand and the corresponding response gesture of the robotic hand. The recorded output voltages of each motion are depicted in Fig. 6(h), and channel 1–4 represent the motions of the index finger, middle finger, ring finger, and the pinkie, respectively. A video demo of the robotic hand control with the finger bending sensors can be found in Video 2 (Supporting information). The amplitude and polarity of the output voltage both control the movement of the robotic fingers. From Fig. 6(g-i–iv), only one finger bends at 90 degrees while the other three remain still, thus only one channel has signals coming from the bending finger. In Fig. 6(g–v), there are output voltages in four channels at the same time due to the synchronized movement of the four fingers. When the hand is grabbing a bottle with a large diameter, four fingers bend at the same time at a small bending angle, hence the output voltage of the sensors is relatively low. While the hand grabs a gracile pen with a smaller diameter, larger output voltages will be generated. If there are more of these arch-shaped sensors incorporated together and placed onto all finger joints, we should be able to differentiate more complex finger motions and hence control the robotic hand more precisely. Therefore, the arch-shaped finger bending sensor has a great potential in real-time control of a robot for diversified applications.

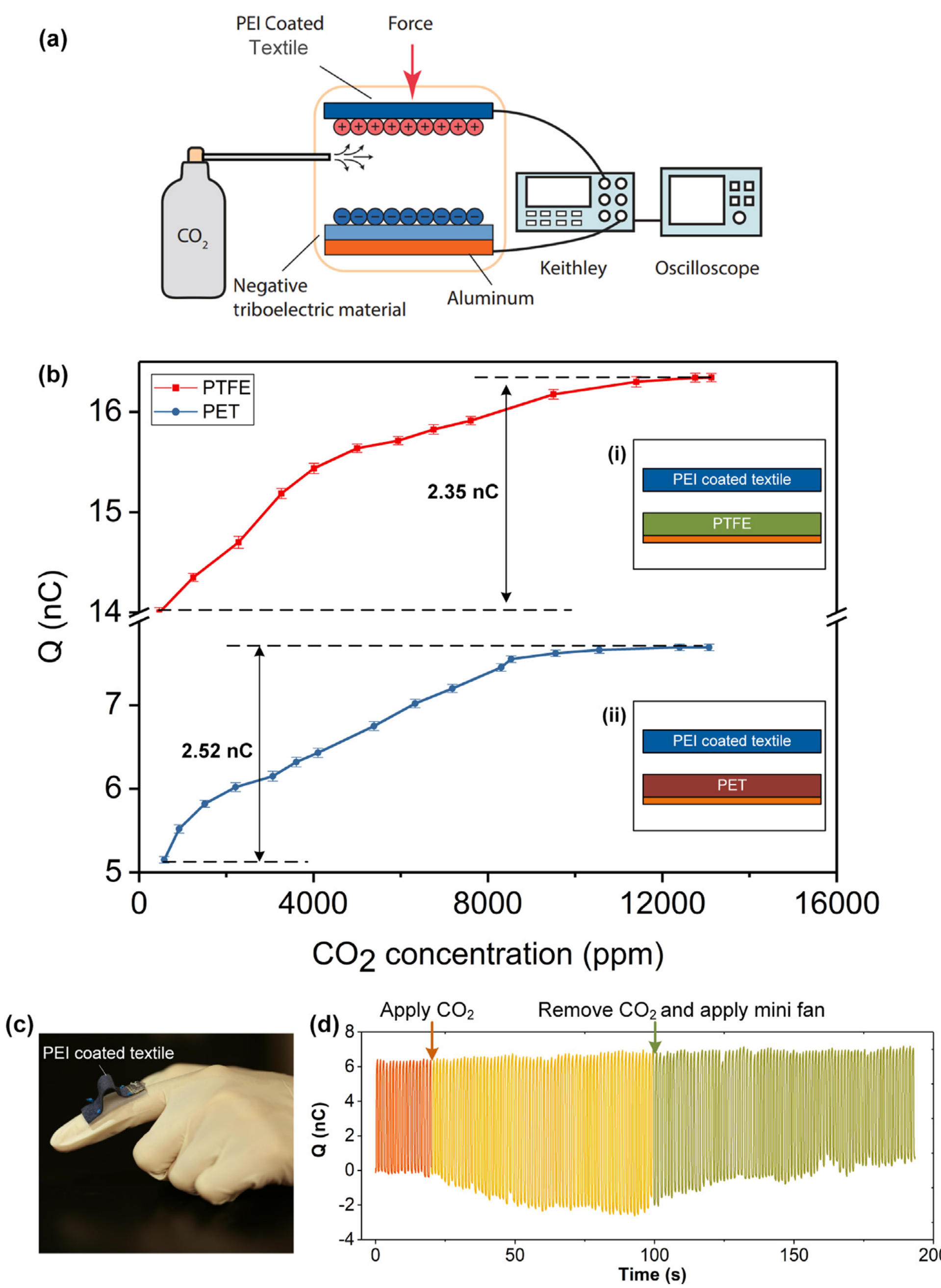

Fig. 8. CO_2 sensing with the textile-based TENG. a) Schematic illustration of the testing set up for CO_2 sensing. b) Response curves of the transferred charge over CO_2 concentration with two different negative triboelectric materials. c) Photograph of the arch-shaped CO_2 sensor mounted on the index finger. d) Dynamic response of the transferred charge over time of the arch-shaped CO_2 sensor.

Supplementary material related to this article can be found online at doi:10.1016/j.nanoen.2018.12.032.

5. Smart textile for healthcare applications

5.1. Activity monitoring

Detection and monitoring of the human actions is an upcoming research area and become ambitious due to the strength of support in healthcare. It is useful in many applications such as patient monitoring at home and it also relates to the various fields of studies such as human-computer interface, medicine or sociology. Four PEDOT:PSS functionalized textile-based TENGs with varying configurations are attached to different body parts for activity monitoring as shown in Fig. 7(a–d). The output voltages of the four devices are recorded with an oscilloscope through the 100 MΩ probes from channel 1 to channel 4. A video demo of the human activity monitoring can be found in Video 3 (Supporting Information).

When the monitored person stands up from a chair, a positive peak voltage is generated in channel 1 due to the separation of the textile and the PTFE thin film. Then, when the person starts to walk at a steady pace, device 2 will generate a repetitive positive and negative peak voltages in channel 2 synchronized with the swinging of the right arm. Hence a higher frequency output can be observed when the person is walking fast. Besides, since the walking motions only involve minor elbow bending, the output voltage from device 3 is quite small at this condition. Furthermore, when the person is running, the frequency of the output is further boosted than fast walking, and the bending motion of the elbow is more evident which contributes to a significant output in channel 3. Besides, in a full cycle of arm swinging forward and backward during running, swinging forward gives a larger contact force in device 2 than swinging backward, which can also be observed from the output voltage in channel 2. Both the two distinct parameters help us differentiate between walking and running, whose speed can be determined from the output frequency. In addition, when the person is exercising through lift weights or other forms of exercise related to arm bending, the multi-arch strain sensor is able to record and track the motions of the arm. As depicted in Fig. 7(e), a higher frequency output voltage is generated when the monitored arm bends fast. Through the monitoring of the bending angle and the moving speed of the arm, we are able to collect the useful information of the exercise. If the person suddenly falls down when he is walking or running, an enormous large positive peak voltage can be detected form device 4. This could be used as a fall detection sensor for the elderly or the disabled. A wireless transmitting module could be implemented to set up an alarm to inform the hospital or the emergency contact if the person did not stand up for a short period. A negative output voltage can only be detected when the person stands up from the ground. Finally, after a consecutive exercise, the person is tired and needs to take a rest, and a negative output voltage is generated when the person sits down on a chair. In short, the four-device-based sensing platform is able to monitor versatile daily activities of a person and even detect a fall, and this real-time and continuous-monitoring information could be highly benefited and essential for a doctor to evaluate a person's health condition. Besides, it may also be helpful for a person to monitor his daily amount of exercise.

5.2. CO_2 sensing

The triboelectric mechanism has been demonstrated to be an effective approach for self-powered gas sensing. The textile could give rise to a higher sensitivity than thin film due to its natural microstructured surface which results in a larger contact area. Distinguished from the plain thin film, the textile also owns another advantage that the detecting gas can reach the contact surface from almost all directions since it is air-permeable. To demonstrate the potential of the textile-based TENG as a CO_2 sensor, polyethylenimine (PEI) solution was spray coated onto the PEDOT:PSS functionalized textile surface. Here the PEI coating becomes the triboelectric layer to generate triboelectric charges, and PEDOT:PSS works only as a conductive electrode for charge collection and transfer. Hence the cotton fabric is coated with non-diluted PEDOT:PSS solution in this section to achieve a better conductivity. The PEI gel was diluted by 10 fold with DI water for spray coating. The size of the PEDOT:PSS functionalized textile was fixed at 4 cm by 4 cm, and the nozzle of the spray bottle sits 5 cm away in the front of the textile central point. Each sample went through 5 sprays of the PEI solution in total. After PEI coating, the textiles were put into the oven with a temperature set at 70 ^{0}C for 30 min until they were fully dried.

The testing set up is shown in Fig. 8(a), where the PEI coated textile is attached to the controllable moving stage, and a negative triboelectric material with an aluminum electrode on the back is attached to the fixed stage right beneath the textile. A commercial CO_2 meter was put beside the triboelectric negative material fixed on the stage for calibration. The whole testing system was sealed with plastic films and a tube inlet was inserted to flow in CO_2 gas. The other side of the tube inlet was connected to the gas tank through a gas flow control meter. The frequency of the moving stage was set as 0.5 Hz and the force was set as 10 N, with the displacement amplitude of 2 cm. The humidity of the environment was 55%.

The transferred charge of the textile-based triboelectric sensor under different CO_2 concentration is measured. With the absorption of CO_2, a carbamate layer which is a CO_2-PEI complexation will be formed and in turn, changing the electronegativity of the PEI layer [41]. This electronegativity change can be projected on the transferred charge of the TENG. The transferred charge with a varying CO_2 concentration of the textile-based TENG with the triboelectric negative material of PTFE and PET is plotted in Fig. 8(b). The red line represents the charge response of the TENG with PTFE as negative material as shown from the inset i in Fig. 8(b), and the blue line indicates the charge response over CO_2 concentration of the TENG demonstrated as inset ii. It can be seen that the transferred charge increases with CO_2 concentration and it almost saturates when the CO_2 concentration reaches 10,000 ppm for both devices. The overall charge variation of the two devices is similar, and the charge changing trends of the two curves are also comparable. The sensitivities of the two devices from 500 ppm to 9000 ppm are calculated based on the testing data in Fig. 8(b), which are 2.69×10^{-4} nC ppm^{-1} for the PTFE-based TENG and 2.54×10^{-4} nC ppm^{-1} for the PET-based TENG. It can be observed that the substitute of the negative material from PTFE to PET wouldn't influence the response curve of the transferred charge much. Instead, since PTFE owns a higher ranking in the triboelectric series than PET, the baseline of the response curve is shifted down. Hence, the PEI coated textile could be used in diversified device configurations with varying required negative triboelectric materials.

Compared to previous work [41], the transferred charge of this textile-based CO_2 sensor didn't decline after 6250 ppm due to the thinner PEI coating, which attributes to a wider sensing range. The detailed explanation is presented in Note S1 (Supporting information). Furthermore, the sensitivity has been improved by means of the microstructures of the textile compared to 2.28×10^{-4} nC ppm^{-1} for 53% RH achieved in the previous work. Although the sensitivity of this triboelectric based CO_2 sensor is not very good, the aim of such wearable CO_2 sensor is not to measure the precise CO_2 concentration. Instead, it is to provide a rough measurement of the CO_2 concentration in the surrounding environment to indicate the indoor air quality or to trigger an alarm when the CO_2 concentration exceeds a threshold value that may danger a human's life. A wearable CO_2 detector can be carried by the user to anywhere to provide a continuous monitoring of the CO_2 concentration in the surrounding environment of the user. Besides, it can also track the user's individual CO_2 exposure over an extended period of time, which is tightly related to human's health status, where the wearability or portability is highly essential.

An arch-shaped CO_2 sensor based on the PEI coated textile and the silicone rubber thin film was fabricated and tested on the human finger. The device configuration and dimension are the same with the finger bending sensor located at the PIP, but the functionalized textile here was coated with non-diluted PEDOT: PSS solution first and then spray coated with 10% PEI solution as shown in Fig. 8(c). The arch-shaped CO_2 sensor then was attached to the PIP joint of the index finger, which bends at 90 degrees repetitively at a frequency of 1 Hz. The commercial CO_2 meter was put beside the wearable CO_2 sensor for the approximate measurement of the CO_2 concentration. A gas tube with another side connected to the CO_2 tank through the gas flow control meter was approached near the arch-shaped CO_2 sensor after 20 s. A video demo of the dynamic response measurement with the arch-shaped CO_2 sensor can be found in Video 4 (Supporting Information). After 100 s, the tube was removed from the sensor and a mini fan was applied for a better ventilation. The dynamic CO_2 sensing response of it is plotted in Fig. 8(d). An almost instant increasement of the charge can be observed when the CO_2 was applied, and a clear drop of the transferred charge could also be seen at 100 s when the CO_2 inlet was removed and the mini fan was applied simultaneously. After 160 s, the transferred charge of the TENG returns to its initial value. This wearable arch-shaped CO_2 sensor could be used to detect and monitor the CO_2 concentration in the environment especially in small space and alarm people when the CO_2 concentration is too high that may threaten human life. Moreover, with a substitute of different functioning materials that are capable of trapping other gas molecules for coating, the functionalized textile could be used to sense other gases for a more comprehensive environmental monitoring.

Supplementary material related to this article can be found online at doi:10.1016/j.nanoen.2018.12.032.

6. Conclusion

In this study, a versatile smart textile for diversified wearable applications is fabricated with a facile and low-cost process which is highly compatible with large-scale fabrication. The triboelectric property of the textile is optimized and its energy harvesting property is investigated. A maximum output power of 3.26 mW is achieved from foot stepping at 2 Hz on a layer of PEDOT: PSS coated textile of $4 \times 4\,cm^2$. It refers to a power density of $2\,W\,m^{-2}$ harvested from human walking at 2 Hz with the smart textile-based TENG, and the matching impedance of the TENG is as low as 14 MΩ. A height-varying multi-arch strain sensor based on the smart textile with a broadened sensing range from 10% to 160% is developed. By leveraging this arch-shaped strain sensor on human fingers, we can successfully monitor finger motions aiming at applications of hand gesture detection for American Sign Language translation and robotic control. Besides, four self-powered sensors based on the smart textiles are fabricated and attached to different parts of the human body for activity monitoring. Together they are able to detect activities such as standing up, walking, running, arm bending, a sudden fall, and sitting. In addition, the smart textile can also be used for CO_2 sensing with the PEI coating, and a wearable arch-shaped CO_2 sensor based on the smart textile on top of a finger is developed. Looking forward, this smart textile could be incorporated into real clothes to function as an energy harvester and all kinds of physical sensors and even gas sensors for healthcare monitoring applications.

7. Experimental section

7.1. Fabrication of the strain sensor

The PEDOT:PSS functionalized textile was first fabricated with the dip coating method. Here the PEDOT:PSS solution was diluted by DI water to a weight percentage of 12.5% in the coating solution. The next step was to prepare the silicone rubber thin films. After dispensing required amounts of Parts A and B of the EcoFlex™ 00–30 into a mixing container (1A:1B by volume or weight), the blend was mixed thoroughly for 3 min and poured into the mold for thin film casting followed by a 20-min baking at 70 °C for curing. Lastly, the arch shape was created by fixing the textile onto the silicone rubber thin film with designed spacing for both textile and silicone rubber by stitching.

7.2. Characterization of the energy harvester and the textile-based sensors

Open-circuit voltage, short-circuit current, and transferred charge measurement were conducted by connecting the output signal to a Keithley Electrometer (Model 6514), and the signals are displayed and recorded with a DSO-X3034A oscilloscope (Agilent). Other voltage measurements were conducted by connecting the output signal directly to a DSO-X3034A oscilloscope (Agilent) with a high impedance probe of 100 MΩ or the normal 1 MΩ probe. For measuring the CO_2 concentration, a commercial CO_2 meter was fixed beside the textile-based CO_2 sensors. To generate stretching motion with controllable speed and maximum strain, a linear motor connected to a programmable Arduino UNO was used.

Acknowledgements

T.H. and Q.S. contributed equally to this work. This work was supported by HiFES Seed Funding-2017-01 grant (R-263-501-012-133) “Hybrid Integration of Flexible Power Source and Pressure Sensors” at the National University of Singapore; Faculty Research Committee (FRC) grant (R-263-000-B56-112) “Thermoelectric power generator (TEG) based self-powered ECG plaster-System integration (Part 3)” at the National University of Singapore, Singapore. T.H. would like to appreciate the support from NUS Suzhou Research Institute (NUSRI) scholarship program for her Ph.D. study.

Appendix A. Supporting information

Supplementary data associated with this article can be found in the online version at doi:10.1016/j.nanoen.2018.12.032.

References

[1] M.L. Hammock, A. Chortos, B.C.K. Tee, J.B.H. Tok, Z. Bao, 25th anniversary article: the evolution of electronic skin (E-Skin): a brief history, design considerations, and recent progress, Adv. Mater. 25 (2013) 5997–6038, https://doi.org/10.1002/adma.201302240.
[2] Y. Cheng, R. Wang, K.H. Chan, X. Lu, J. Sun, G.W. Ho, A. Biomimetic, Conductive tendril for ultrastretchable and integratable electronics, muscles, and sensors, ACS Nano 12 (2018) 3898–3907, https://doi.org/10.1021/acsnano.8b01372.
[3] Y.T. Jao, P.K. Yang, C.M. Chiu, Y.J. Lin, S.W. Chen, D. Choi, Z.H. Lin, A textile-based triboelectric nanogenerator with humidity-resistant output characteristic and its applications in self-powered healthcare sensors, Nano Energy 50 (2018) 513–520, https://doi.org/10.1016/j.nanoen.2018.05.071.
[4] C.H. Chen, P.W. Lee, Y.H. Tsao, Z.H. Lin, Utilization of self-powered electrochemical systems: metallic nanoparticle synthesis and lactate detection, Nano Energy 42 (2017) 241–248, https://doi.org/10.1016/j.nanoen.2017.10.064.
[5] J. Bian, N. Wang, J. Ma, Y. Jie, J. Zou, X. Cao, Stretchable 3D polymer for simultaneously mechanical energy harvesting and biomimetic force sensing, Nano Energy 47 (2018) 442–450, https://doi.org/10.1016/j.nanoen.2018.03.027.
[6] J. Zhong, Q. Zhong, X. Zang, N. Wu, W. Li, Y. Chu, L. Lin, Nano energy flexible PET / EVA-based piezoelectret generator for energy harvesting in harsh environments, Nano Energy 37 (2017) 268–274, https://doi.org/10.1016/j.nanoen.2017.05.034.
[7] S. Han, J. Kim, S.M. Won, Y. Ma, D. Kang, Z. Xie, K.T. Lee, H.U. Chung, A. Banks, S. Min, S.Y. Heo, C.R. Davies, J.W. Lee, C.H. Lee, B.H. Kim, K. Li, Y. Zhou, C. Wei, X. Feng, Y. Huang, J.A. Rogers, Battery-free, wireless sensors for full-body pressure and temperature mapping, Sci. Transl. Med. 10 (2018) eaan4950, https://doi.org/10.1126/scitranslmed.aan4950.
[8] Y. Liu, J.J.S. Norton, R. Qazi, Z. Zou, K.R. Ammann, H. Liu, L. Yan, P.L. Tran, K.I. Jang, J.W. Lee, D. Zhang, K.A. Kilian, S.H. Jung, T. Bretl, J. Xiao, M.J. Slepian, Y. Huang, J.W. Jeong, J.A. Rogers, Epidermal mechano-acoustic sensing electronics for cardiovascular diagnostics and human-machine interfaces, Sci. Adv. 2 (2016) e1601185, https://doi.org/10.1126/sciadv.1601185.
[9] W. Gao, S. Emaminejad, H.Y.Y. Nyein, S. Challa, K. Chen, A. Peck, H.M. Fahad, H. Ota, H. Shiraki, D. Kiriya, D.H. Lien, G.A. Brooks, R.W. Davis, A. Javey, Fully

integrated wearable sensor arrays for multiplexed in situ perspiration analysis, Nature 529 (2016) 509–514, https://doi.org/10.1038/nature16521.
[10] Z. Wu, W. Ding, Y. Dai, K. Dong, C. Wu, L. Zhang, Z. Lin, J. Cheng, Z.L. Wang, Self-powered multifunctional motion sensor enabled by magnetic regulated triboelectric nanogenerator, ACS Nano 12 (2018) 5726–5733, https://doi.org/10.1021/acsnano.8b01589.
[11] T. Bu, T. Xiao, Z. Yang, G. Liu, X. Fu, J. Nie, T. Guo, Y. Pang, J. Zhao, F. Xi, C. Zhang, Z.L. Wang, Stretchable triboelectric–photonic smart skin for tactile and gesture sensing, Adv. Mater. 30 (2018) 1800066, https://doi.org/10.1002/adma.201800066.
[12] L. Li, Y. Bai, L. Li, S. Wang, T. Zhang, A. Superhydrophobic Smart, Coating for flexible and wearable sensing electronics, Adv. Mater. 29 (2017) 1702517, https://doi.org/10.1002/adma.201702517.
[13] X. Wang, Y. Gu, Z. Xiong, Z. Cui, T. Zhang, Silk-molded flexible, ultrasensitive, and highly stable electronic skin for monitoring human physiological signals, Adv. Mater. 26 (2014) 1336–1342, https://doi.org/10.1002/adma.201304248.
[14] H. Liu, C. Lee, T. Kobayashi, C.J. Tay, C. Quan, Investigation of a MEMS piezoelectric energy harvester system with a frequency-widened-bandwidth mechanism introduced by mechanical stoppers, Smart Mater. Struct. 21 (2012) 035005, https://doi.org/10.1088/0964-1726/21/3/035005.
[15] J.-H. Lee, J.Y. Park, E.B. Cho, T.Y. Kim, S.A. Han, T.-H. Kim, Y. Liu, S.K. Kim, C.J. Roh, H.-J. Yoon, H. Ryu, W. Seung, J.S. Lee, J. Lee, S.-W. Kim, Reliable piezoelectricity in bilayer WSe_2 for piezoelectric nanogenerators, Adv. Mater. 29 (2017) 1606667, https://doi.org/10.1002/adma.201606667.
[16] S.A. Han, T.-H. Kim, S.K. Kim, K.H. Lee, H.-J. Park, J.-H. Lee, S.-W. Kim, Point-defect-passivated MoS_2 nanosheet-based high performance piezoelectric nanogenerator, Adv. Mater. 30 (2018) 1800342, https://doi.org/10.1002/adma.201800342.
[17] Q. Zheng, B. Shi, Z. Li, Z.L. Wang, Recent progress on piezoelectric and triboelectric energy harvesters in biomedical systems, Adv. Sci. 4 (2017) 1700029, https://doi.org/10.1002/advs.201700029.
[18] Y. Ji, K. Zhang, Y. Yang, A one-structure-based multieffects coupled nanogenerator for simultaneously scavenging thermal, solar, and mechanical energies, Adv. Sci. 5 (2018) 1700622, https://doi.org/10.1002/advs.201700622.
[19] Y. Chu, J. Zhong, H. Liu, Y. Ma, N. Liu, Y. Song, J. Liang, Z. Shao, Y. Sun, Y. Dong, X. Wang, L. Lin, Human pulse diagnosis for medical assessments using a wearable piezoelectret sensing system, Adv. Funct. Mater. 28 (2018) 1803413, https://doi.org/10.1002/adfm.201803413.
[20] H. Song, I. Karakurt, M. Wei, N. Liu, Y. Chu, J. Zhong, L. Lin, Lead iodide nanosheets for piezoelectric energy conversion and strain sensing, Nano Energy 49 (2018) 7–13, https://doi.org/10.1016/j.nanoen.2018.04.029.
[21] H. Ouyang, J. Tian, G. Sun, Y. Zou, Z. Liu, H. Li, L. Zhao, B. Shi, Y. Fan, Y. Fan, Z.L. Wang, Z. Li, Self-powered pulse sensor for antidiastole of cardiovascular disease, Adv. Mater. 29 (2017) 1703456, https://doi.org/10.1002/adma.201703456.
[22] S. Cheon, H. Kang, H. Kim, Y. Son, J.Y. Lee, H.J. Shin, S.W. Kim, J.H. Cho, High-performance triboelectric nanogenerators based on electrospun polyvinylidene fluoride–silver nanowire composite nanofibers, Adv. Funct. Mater. 28 (2018) 1703778, https://doi.org/10.1002/adfm.201703778.
[23] X. Chen, Y. Wu, A. Yu, L. Xu, L. Zheng, Y. Liu, H. Li, Z. Lin Wang, Self-powered modulation of elastomeric optical grating by using triboelectric nanogenerator, Nano Energy 38 (2017) 91–100, https://doi.org/10.1016/j.nanoen.2017.05.039.
[24] H.J. Yoon, H. Ryu, S.W. Kim, Sustainable powering triboelectric nanogenerators: approaches and the path towards efficient use, Nano Energy 51 (2018) 270–285, https://doi.org/10.1016/j.nanoen.2018.06.075.
[25] Y. Chen, Y. Jie, J. Wang, J. Ma, X. Jia, W. Dou, X. Cao, Triboelectrification on natural rose petal for harvesting environmental mechanical energy, Nano Energy 50 (2018) 441–447, https://doi.org/10.1016/j.nanoen.2018.05.021.
[26] X. Chen, X. Pu, T. Jiang, A. Yu, L. Xu, Z.L. Wang, Tunable optical modulator by coupling a triboelectric nanogenerator and a dielectric elastomer, Adv. Funct. Mater. 27 (2017) 1603788, https://doi.org/10.1002/adfm.201603788.
[27] R. Hinchet, A. Ghaffarinejad, Y. Lu, J.Y. Hasani, S.W. Kim, P. Basset, Understanding and modeling of triboelectric-electret nanogenerator, Nano Energy 47 (2018) 401–409, https://doi.org/10.1016/j.nanoen.2018.02.030.
[28] J. Chen, H. Guo, X. Pu, X. Wang, Y. Xi, C. Hu, Traditional weaving craft for one-piece self-charging power textile for wearable electronics, Nano Energy 50 (2018) 536–543, https://doi.org/10.1016/j.nanoen.2018.06.009.
[29] L. Feng, G. Liu, H. Guo, Q. Tang, X. Pu, J. Chen, X. Wang, Y. Xi, C. Hu, Hybridized nanogenerator based on honeycomb-like three electrodes for efficient ocean wave energy harvesting, Nano Energy 47 (2018) 217–223, https://doi.org/10.1016/j.nanoen.2018.02.042.
[30] X. Wang, Y. Yang, Effective energy storage from a hybridized electromagnetic-triboelectric nanogenerator, Nano Energy 32 (2017) 36–41, https://doi.org/10.1016/j.nanoen.2016.12.006.
[31] H. Hou, Q. Xu, Y. Pang, L. Li, J. Wang, C. Zhang, C. Sun, Efficient storing energy harvested by triboelectric nanogenerators using a safe and durable all-solid-state sodium-ion battery, Adv. Sci. 4 (2017) 1700072, https://doi.org/10.1002/advs.201700072.
[32] Z. Yuan, X. Du, N. Li, Y. Yin, R. Cao, X. Zhang, S. Zhao, H. Niu, T. Jiang, W. Xu, Z.L. Wang, C. Li, Triboelectric-based transparent secret code, Adv. Sci. 5 (2018) 1700881, https://doi.org/10.1002/advs.201700881.
[33] X. Pu, M. Liu, L. Li, C. Zhang, Y. Pang, C. Jiang, L. Shao, W. Hu, Z.L. Wang, Efficient charging of Li-ion batteries with pulsed output current of triboelectric nanogenerators, Adv. Sci. 3 (2015) 1500255, https://doi.org/10.1002/advs.201500255.
[34] S.Y. Kuang, G. Zhu, Z.L. Wang, Triboelectrification-enabled self-powered data storage, Adv. Sci. 5 (2018) 1700658, https://doi.org/10.1002/advs.201700658.
[35] S. Chen, N. Wang, L. Ma, T. Li, M. Willander, Y. Jie, X. Cao, Z.L. Wang, Triboelectric nanogenerator for sustainable wastewater treatment via a self-powered electrochemical process, Adv. Energy Mater. 6 (2016) 1501778, https://doi.org/10.1002/aenm.201501778.
[36] R.K. Gupta, Q. Shi, L. Dhakar, T. Wang, C.H. Heng, C. Lee, Broadband energy harvester using non-linear polymer spring and electromagnetic/triboelectric hybrid mechanism, Sci. Rep. 7 (2017) 41396, https://doi.org/10.1038/srep41396.
[37] Q. Shi, H. Wang, H. Wu, C. Lee, Self-powered triboelectric nanogenerator buoy ball for applications ranging from environment monitoring to water wave energy farm, Nano Energy 40 (2017) 203–213, https://doi.org/10.1016/j.nanoen.2017.08.018.
[38] L. Dhakar, S. Gudla, X. Shan, Z. Wang, F.E.H. Tay, C.H. Heng, C. Lee, Large scale triboelectric nanogenerator and self-powered pressure sensor array using low cost roll-to-roll UV embossing, Sci. Rep. 6 (2016) 22253, https://doi.org/10.1038/srep22253.
[39] Q. Shi, H. Wu, H. Wang, H. Wu, C. Lee, Self-powered gyroscope ball using a triboelectric mechanism, Adv. Energy Mater. 7 (2017) 1701300, https://doi.org/10.1002/aenm.201701300.
[40] Q. Shi, H. Wang, T. Wang, C. Lee, Self-powered liquid triboelectric microfluidic sensor for pressure sensing and finger motion monitoring applications, Nano Energy 30 (2016) 450–459.
[41] H. Wang, H. Wu, D. Hasan, T. He, Q. Shi, C. Lee, Self-powered dual-mode amenity sensor based on the water-air triboelectric nanogenerator, ACS Nano 11 (2017) 10337–10346, https://doi.org/10.1021/acsnano.7b05213.
[42] S. Lee, H. Wang, Q. Shi, L. Dhakar, J. Wang, N.V. Thakor, S.C. Yen, C. Lee, Development of battery-free neural interface and modulated control of tibialis anterior muscle via common peroneal nerve based on triboelectric nanogenerators (TENGs), Nano Energy 33 (2017) 1–11, https://doi.org/10.1016/j.nanoen.2016.12.038.
[43] Y. Wang, C. Zhu, R. Pfattner, H. Yan, L. Jin, S. Chen, F. Molina-Lopez, F. Lissel, J. Liu, N.I. Rabiah, Z. Chen, J.W. Chung, C. Linder, M.F. Toney, B. Murmann, Z. Bao, A highly stretchable, transparent, and conductive polymer, Sci. Adv. 3 (2017) e1602076, https://doi.org/10.1126/sciadv.1602076.
[44] G. Cai, J. Wang, K. Qian, J. Chen, S. Li, P.S. Lee, Extremely stretchable strain sensors based on conductive self-healing dynamic cross-links hydrogels for human-motion detection, Adv. Sci. 4 (2017) 1600190, https://doi.org/10.1002/advs.201600190.
[45] X. He, Y. Zi, H. Guo, H. Zheng, Y. Xi, C. Wu, J. Wang, W. Zhang, C. Lu, Z.L. Wang, A highly stretchable fiber-based triboelectric nanogenerator for self-powered wearable electronics, Adv. Funct. Mater. 27 (2017) 1604378, https://doi.org/10.1002/adfm.201604378.
[46] Z. Su, H. Wu, H. Chen, H. Guo, X. Cheng, Y. Song, X. Chen, H. Zhang, Digitalized self-powered strain gauge for static and dynamic measurement, Nano Energy 42 (2017) 129–137, https://doi.org/10.1016/j.nanoen.2017.10.004.
[47] Y. Wang, Y. Wang, Y. Yang, Graphene–polymer nanocomposite-based redox-induced electricity for flexible self-powered strain sensors, Adv. Energy Mater. 8 (2018) 1800961, https://doi.org/10.1002/aenm.201800961.
[48] Q. Shen, X. Xie, M. Peng, N. Sun, H. Shao, H. Zheng, Z. Wen, X. Sun, Self-powered vehicle emission testing system based on coupling of triboelectric and chemoresistive effects, Adv. Funct. Mater. 28 (2018) 1703420, https://doi.org/10.1002/adfm.201703420.
[49] Y. Su, G. Xie, H. Tai, S. Li, B. Yang, S. Wang, Q. Zhang, H. Du, H. Zhang, X. Du, Y. Jiang, Self-powered room temperature NO_2 detection driven by triboelectric nanogenerator under UV illumination, Nano Energy 47 (2018) 316–324, https://doi.org/10.1016/j.nanoen.2018.02.031.
[50] S. Cui, Y. Zheng, T. Zhang, D. Wang, F. Zhou, W. Liu, Self-powered ammonia nanosensor based on the integration of the gas sensor and triboelectric nanogenerator, Nano Energy 49 (2018) 31–39, https://doi.org/10.1016/j.nanoen.2018.04.033.
[51] J. Hu, H. Meng, G. Li, S.I. Ibekwe, A review of stimuli-responsive polymers for smart textile applications, Smart Mater. Struct. 21 (2012) 053001, https://doi.org/10.1088/0964-1726/21/5/053001.
[52] J. Lee, H. Kwon, J. Seo, S. Shin, J.H. Koo, C. Pang, S. Son, J.H. Kim, Y.H. Jang, D.E. Kim, T. Lee, Conductive fiber-based ultrasensitive textile pressure sensor for wearable electronics, Adv. Mater. 27 (2015) 2433–2439, https://doi.org/10.1002/adma.201500009.
[53] J. Ge, L. Sun, F.R. Zhang, Y. Zhang, L.A. Shi, H.Y. Zhao, H.W. Zhu, H.L. Jiang, S.H. Yu, A stretchable electronic fabric artificial skin with pressure-, lateral strain-, and flexion-sensitive properties, Adv. Mater. 28 (2016) 722–728, https://doi.org/10.1002/adma.201504239.
[54] Y.-C. Lai, J. Deng, S.L. Zhang, S. Niu, H. Guo, Z.L. Wang, Single-thread-based wearable and highly stretchable triboelectric nanogenerators and their applications in cloth-based self-powered human-interactive and biomedical sensing, Adv. Funct. Mater. 27 (2017) 1604462.
[55] K. Dong, J. Deng, Y. Zi, Y.C. Wang, C. Xu, H. Zou, W. Ding, Y. Dai, B. Gu, B. Sun, Z.L. Wang, 3D orthogonal woven triboelectric nanogenerator for effective biomechanical energy harvesting and as self-powered active motion sensors, Adv. Mater. 29 (2017) 1702648, https://doi.org/10.1002/adma.201702648.
[56] X. Li, Z.H. Lin, G. Cheng, X. Wen, Y. Liu, S. Niu, Z.L. Wang, 3D fiber-based hybrid nanogenerator for energy harvesting and as a self-powered pressure sensor, ACS Nano 8 (2014) 10674–10681, https://doi.org/10.1021/nn504243j.
[57] S.L. Zhang, Y.C. Lai, X. He, R. Liu, Y. Zi, Z.L. Wang, Auxetic foam-based contact-mode triboelectric nanogenerator with highly sensitive self-powered strain sensing capabilities to monitor human body movement, Adv. Funct. Mater. 27 (2017) 1606695, https://doi.org/10.1002/adfm.201606695.
[58] Z. Wen, M.H. Yeh, H. Guo, J. Wang, Y. Zi, W. Xu, J. Deng, L. Zhu, X. Wang, C. Hu, L. Zhu, X. Sun, Z.L. Wang, Self-powered textile for Wearable electronics by hybridizing fiber-shaped nanogenerators, solar cells, and supercapacitors, Sci. Adv. 2 (2016) e1600097, https://doi.org/10.1126/sciadv.1600097.
[59] J. Xiong, M.F. Lin, J. Wang, S.L. Gaw, K. Parida, P.S. Lee, Wearable all-fabric-based

triboelectric generator for water energy harvesting, Adv. Energy Mater. 7 (2017) 1701243, https://doi.org/10.1002/aenm.201701243.
[60] X. Pu, L. Li, M. Liu, C. Jiang, C. Du, Z. Zhao, W. Hu, Z.L. Wang, Wearable self-charging power textile based on flexible yarn supercapacitors and fabric nanogenerators, Adv. Mater. 28 (2016) 98–105, https://doi.org/10.1002/adma.201504403.
[61] M. Liu, X. Pu, C. Jiang, T. Liu, X. Huang, L. Chen, C. Du, J. Sun, W. Hu, Z.L. Wang, Large-area all-textile pressure sensors for monitoring human motion and physiological signals, Adv. Mater. 29 (2017) 1703700, https://doi.org/10.1002/adma.201703700.
[62] H. Shi, C. Liu, Q. Jiang, J. Xu, Effective approaches to improve the electrical conductivity of PEDOT: PSS: a review, Adv. Electron. Mater. 1 (2015) 1500017, https://doi.org/10.1002/aelm.201500017.
[63] H. Yan, S. Arima, Y. Mori, T. Kagata, H. Sato, H. Okuzaki, Poly (3, 4-ethylenedioxythiophene)/poly (4-styrenesulfonate): Correlation between colloidal particles and thin films, Thin Solid Films 517 (2009) 3299–3303, https://doi.org/10.1016/j.tsf.2009.01.004.
[64] J. Lee, D. Han, H. Shin, S. Yeom, B. Ju, W. Lee, PEDOT: PSS-based temperature-detection thread for wearable devices, Sensors 18 (2018) 2996, https://doi.org/10.3390/s18092996.
[65] Z. Fan, P. Li, D. Du, J. Ouyang, Significantly enhanced thermoelectric properties of PEDOT:PSS films through sequential post-treatments with common acids and bases, Adv. Energy Mater. 7 (2017) 1602116, https://doi.org/10.1002/aenm.201602116.
[66] Y. Ding, M.A. Invernale, G.A. Sotzing, Conductivity trends of PEDOT-PSS impregnated fabric and the effect of conductivity on electrochromic textile, ACS Appl. Mater. Interfaces 2 (2010) 1588–1593, https://doi.org/10.1021/am100036n.
[67] Z. Wen, Y. Yang, N. Sun, G. Li, Y. Liu, C. Chen, J. Shi, L. Xie, H. Jiang, D. Bao, Q. Zhuo, X. Sun, wrinkled PEDOT:PSS film based stretchable and transparent triboelectric nanogenerator for wearable energy harvesters and active motion sensors, Adv. Funct. Mater. 28 (2018) 1803684, https://doi.org/10.1002/adfm.201803684.
[68] Y. Kim, J. Na, C. Park, H. Shin, E. Kim, PEDOT as a flexible organic electrode for a thin film acoustic energy harvester, ACS Appl. Mater. Interfaces 7 (2015) 16279–16286, https://doi.org/10.1021/acsami.5b02762.
[69] J. Zhong, Q. Zhong, Q. Hu, N. Wu, W. Li, B. Wang, B. Hu, J. Zhou, Stretchable self-powered fiber-based strain sensor, Adv. Funct. Mater. 25 (2015) 1798–1803, https://doi.org/10.1002/adfm.201404087.
[70] T. Lee, W. Lee, S.W. Kim, J.J. Kim, B.S. Kim, Flexible textile strain wireless sensor functionalized with hybrid carbon nanomaterials supported ZnO nanowires with controlled aspect ratio, Adv. Funct. Mater. 26 (2016) 6206–6214, https://doi.org/10.1002/adfm.201601237.

Tianyiyi He received her B.Eng. degree from the School of Microelectronics and Solid-state Electronics at the University of Electronic Science and Technology of China (UESTC), Chengdu, China, in 2016. She is now a Ph.D. candidate in the Department of Electrical and Computer Engineering, National University of Singapore. Her research interests include energy harvesters, triboelectric nanogenerator, thermoelectric energy harvester, and self-powered sensors.

Qiongfeng Shi received his B.Eng. degree from the Department of Electronic Engineering and Information Science, University of Science and Technology of China (USTC) in 2012, and received his Ph.D. degree from the Department of Electrical and Computer Engineering, National University of Singapore (NUS) in 2018. He is currently a Research Fellow in the Department of Electrical and Computer Engineering, National University of Singapore. His research interests include energy harvesters, triboelectric nanogenerator, self-powered sensors, and wearable/implantable electronics.

Hao Wang received Hao Wang received the B.Eng. degree from the School of Optoelectronic Information, University of Electronic Science and Technology of China, in 2010. He is currently pursuing the M.Eng. degree with the Department of Electrical and Computer Engineering. He is also a Research Engineer of Electrical and Computer Engineering with the National University of Singapore. His research interests are focused on nanoneedle devices for transdermal drug delivery.

Wen Feng received her B.Eng. degree in Metallic Materials Engineering from the School of Mechanical and Electric Engineering at Soochow University, Suzhou, China, in 2017. She is now pursuing Ph.D degree at Electrical and Computer Engineering, NUS. She mainly focuses on energy harvesting and wearable sensors.

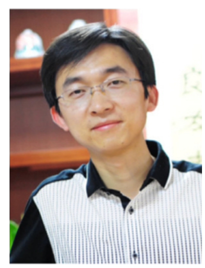

Tao Chen received the B.Sc. degree in Mechanical Design, Manufacturing and Automation, M.Sc. degree in Mechatronic Engineering, and Ph.D. degree in Mechatronic Engineering from Harbin Institute of Technology, Harbin, China, in 2004, 2006, and 2010, respectively. He is a visiting scholar in National University of Singapore in 2018. He is currently an associate professor at Soochow University, Suzhou, China. His main research interests include MEMS, sensors, and actuators.

Jianyong Ouyang received his Ph.D., master and bachelor degrees from the Institute for Molecular Science in Japan, the Institute of Chemistry of the Chinese Academy of Science, and the Tsinghua university in Beijing, respectively. He worked as an assistant professor at the Japanese Advanced Institute of Science and Technology and a postdoctoral researcher at the University of California, Los Angeles (UCLA) before joining the National University of Singapore as an assistant professor in 2006. He was promoted to associate professor in 2012. His research interests include flexible electronics and energy materials and devices.

Chengkuo Lee received his Ph.D. degree in Precision engineering from The University of Tokyo in 1996. Currently, he is the director of Center for Intelligent Sensors and MEMS, and an Associate Professor in the Department of Electrical and Computer Engineering, National University of Singapore, Singapore. In 2001, he cofounded Asia Pacific Microsystems, Inc., where he was the Vice President. From 2006–2009, he was a Senior Member of the Technical Staff at the Institute of Microelectronics, A-STAR, Singapore. He has contributed to more than 300 international conference papers and extended abstracts and 270 peer-reviewed international journal articles.